

# THE ORGANIC AEROSOLS OF TITAN'S ATMOSPHERE

Christophe Sotin<sup>(1)</sup>, Kenneth Lawrence<sup>(1)</sup>, Patricia M. Beauchamp<sup>(1)</sup>, Wayne Zimmerman<sup>(1)</sup>

<sup>(1)</sup>Jet Propulsion Laboratory, California Institute of Technology, 4800 Oak Grove Drive, Pasadena, CA, 91109 (U.S.A.), Christophe.sotin@jpl.nasa.gov

## ABSTRACT

One of Titan's many characteristics is the presence of a haze that veils its surface. This haze is composed of heavy organic particles and determining the chemical composition of these particles is a primary objective for future probes that would conduct in situ analysis. Meanwhile, solar occultations provide constraints on the optical characteristics of the haze layer. This paper describes solar occultation observations obtained by the Visual and Infrared Mapping Spectrometer (VIMS) onboard the Cassini spacecraft. These observations strongly constrain the optical characteristics of the haze layer. We detail the different steps involved in the processing of these data and apply them to two occultations that were observed at the South Pole and at the equator in order to investigate the latitudinal dependence of optical properties. The light curves obtained in seven atmospheric windows between 0.933- $\mu\text{m}$  to 5- $\mu\text{m}$  allow us to characterize atmospheric layers from 300 km to the surface. Very good fits of the light curves are obtained using a simple profile of number density of aerosols that is characterized by a scale height. The main difference between the South Pole and the equator is that the value of the scale height increases with altitude at the South Pole whereas it decreases at the equator. The vertically integrated amount of aerosols is similar at the two locations. The curve describing the cross-section versus wavelength is identical at the two locations suggesting that the aerosols have similar characteristics. Finally, we find that the two-way vertical transmission at 5- $\mu\text{m}$  is as large as 80% at both locations.

## 1. INTRODUCTION

Titan is the only satellite in the solar system with a dense atmosphere with methane constituting the second largest component. Methane is irreversibly transformed into ethane by photolysis. The carbon cycle includes the replenishment of the atmosphere with methane [1,2], the formation of clouds at mid-latitudes [3], the formation of ethane clouds above the North pole during winter [4], the precipitations of methane and ethane [3,4], the formation of organic molecules in the upper atmosphere that are the haze particles [5], the sedimentation of those heavy organic molecules that

are eventually swept by surface winds to form the dunes [6], the formation of lakes at polar latitudes [7] and the interaction of liquid hydrocarbons with the icy porous regolith [2,7]. The aerosols in Titan's atmosphere are of three types: those that form the mid-latitude clouds, those that form the polar clouds [9] and those that are dispersed in the atmosphere and fall on the surface where they provide the material that compose the dunes (Table 1). This paper deals with the later type. The present study uses observations of solar occultation to constrain the optical characteristics and the number density of these particles in Titan's atmosphere.

Although most of the light is absorbed and scattered by atmospheric molecules, the VIMS instrument has demonstrated that Titan's surface can be observed in seven atmospheric windows [16]. These atmospheric windows are 5 spectrally narrow windows at wavelengths smaller than 2.5- $\mu\text{m}$  and 2 wider windows centred at 2.723- and 5.006  $\mu\text{m}$  (Fig. 1). The last one is limited by the spectral range of the detectors and it is probable that the window extends at longer wavelengths. In these windows, only aerosols absorb and scatter light. Solar occultation observations at those wavelengths provide a unique data set that allows us to investigate the optical properties of aerosols.

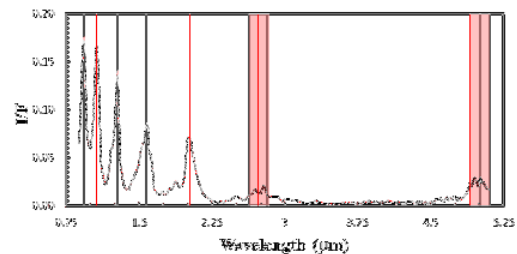


Fig. 1: Typical spectrum of Titan's surface of a bright area known as Adiri. Titan's surface can be observed when I/F have maxima in 5 narrow atmospheric windows and two wider windows in shaded area.

The mass of aerosols in Titan's atmosphere is orders of magnitudes less than the mass of material that makes Titan's dunes. Aerosols are aggregates of about 3,000 monomers [4,5] that are approximately 50 nm in radius [5]. Using a density of 800 kg/m<sup>3</sup>, and ignoring

variations of haze opacity with latitude [13], we find that the total mass of aerosols is 0.07 GT. If the density is scaled by a factor of 2 to account for higher opacity at the equator, then the mass becomes a fraction of GT, but still orders of magnitudes less than the amount of organic particles that compose the dunes that is estimated at more than 200,000 GT of carbon [8]. It must be noted that the vertical maximum value of the number density of particles varies from  $5 \text{ cm}^{-3}$  to  $90 \text{ cm}^{-3}$  (Table 2). The occultation observations described in the present paper provide constraints on this value.

Table 1: List of the VIMS atmospheric windows where Titan’s surface can be observed. The S/N ratio is obtained from the solar spectra as described in section 2.3.

	spectel #	wavelength $\mu\text{m}$	S/N (T10 – 40 ms)
B1	100	0.933	119
B2	108*	1.065	38
B3	121	1.278	227
B4	139	1.574	109
D1	166/167	2.026	371/489
D2	203	2.630	184
	208/209	2.723	193/165
	214	2.816	133
D3	339	4.903	24
	345	5.006	22
	352	5.108	19

\*Spectel #108 has a low S/N of 38. It is better to use spectels #107 (1.0476- $\mu\text{m}$ ) and #109 (1.0818- $\mu\text{m}$ ) which have S/N of 150 and 118, respectively. In D2, spectel #213 (2.7989- $\mu\text{m}$ ) has an S/N of 57 compared to about 150 for the others. For D1, we can also use 6 or 7 detectors. The 6 recommended ones are from 1.985- to 2.068- $\mu\text{m}$ .

Previous work on the density profile of aerosols includes the solar occultation T10 [4] that is used as a reference in the present paper and observations made during the descent of the Huygens probe in Titan’s atmosphere [5]. The Huygens landing site is located at  $10.6^\circ\text{S}$  and the observation of the T53 solar occultation is close to the location of the Huygens Landing Site (HLS). Comparing the density profile with the same instruments will allow us to constrain numerical simulations [13] that suggest that the haze opacity increases by a factor of 3 from the South Pole to the equator, and then decreases by a factor of 2 between  $30^\circ\text{N}$  and the North Pole. These variations may result in different values for the reference density of aerosols. It also allows us to refine the amount of aerosols present in Titan’s atmosphere.

The timescale for the formation of the dunes is on the same order of magnitude as the age of methane in Titan’s atmosphere. Aerosols are formed in the neutral atmosphere in a narrow layer about 40-km thick near an altitude of 400-km altitude [11]. Some aerosols are also formed at much higher altitudes in the ionosphere [7]. Coupled dynamics-microphysics models of Titan’s atmosphere [11] use formation rates between 10- to 100-kg/s. In these models, aerosols form only in the neutral atmosphere. Aerosols formed at higher altitudes at a rate of 3- to 30-kg/s [7] fall and mix with the ones formed at 400 km altitude. These different numbers suggest that the formation rate of aerosols must be comprised between 10 and 130 kg/s. With a value of 0.14 GT of aerosols in the atmosphere, the residence time is equal to 35 and 450 years. The production rate can also be used to assess the time required to form the dunes covering Titan’s surface. With a value of 200,000 GT, this time is between 50- and 630-Myr. This timescale is in rough agreement with the value of 470 Myr for the age of atmospheric methane [14], the recently revised crater retention age between 200 Myr and 1 Gyr [15], and the time necessary to produce the amount of ethane necessary to explain the low value of Titan’s polar radius by subsidence [2]. Determining the amount of aerosols in Titan’s atmosphere and its variability in time and latitude provides new constraints on the global Carbon cycle on Titan.

Table 2: Different types of aerosols in Titan’s atmosphere.

Type of aerosols /particles	Location	Size	number density
<b>haze</b>	Global peak density is around 80 – 100 km	0.2 to a few $\mu\text{m}$ made of 3,000 monomers	$30 \text{ cm}^{-3}$ at 90 km and strong decrease below [3] / Peak value of $5 \text{ cm}^{-3}$ [5]
<b>Ethane clouds</b>	Above 50 deg latitude permanent 40 to 60 km altitude	1 to 3 $\mu\text{m}$	Column abundance of $60,000 \text{ cm}^{-2} = 60 \text{ cm}^{-3}$ if cloud is 10 m thick.
<b>Methane clouds</b>	South mid-latitudes in winter episodic 10 km altitude	Larger than 10 $\mu\text{m}$ [12]	

In section 2, this paper describes the different steps required to process the solar occultation data in order to infer the density profile of aerosols. Results of two occultation observations at the South Pole and at the equator are provided in section 3. The implications for the density profile of aerosols and their optical properties are drawn in section 4.

## 2. PROCESSING SOLAR OCCULTATION DATA

The VIMS instrument is equipped with a solar port that is aligned with the UVIS port in order to observe the Sun, which cannot be done through the instrument's boresight since the sunlight is much too bright. At Saturn, the Sun is about 1 mrad in diameter or twice the nominal field of view (FoV) of the instrument. Therefore a minimum of 8x8 pixel images is usually taken in order to cover the entire Sun. Another constraint is the integration time which has to be large enough to allow some light when probing the deepest layers of the atmosphere yet small enough to avoid saturation before the occultation starts. A smaller integration time and a smaller image size yield better vertical resolution. A trade-off has been found with an integration time of 20- to 40-ms.

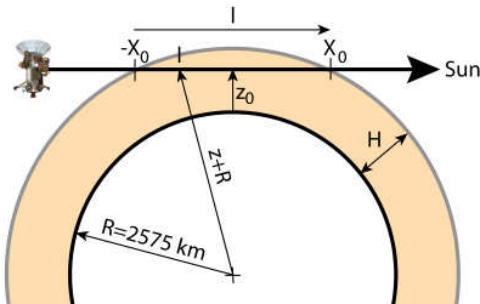


Fig. 2: Sketch illustrating the ray path through Titan's atmosphere in the plane defined by the S/C-Sun vector and Titan's centre. The atmosphere has a thickness,  $H$ , and the impact parameter,  $z_0$ , is the distance closest to Titan along the ray path. The opacity increases as the value of the impact parameter decreases.

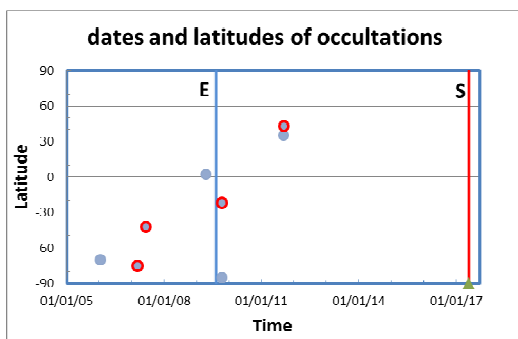


Fig. 3: Latitude and date of the solar occultation observations. The vertical blue and red lines represent the equinox and solstice, respectively. The inclination of the orbit explains the trend from South Polar latitudes at the beginning to Northern latitudes after the equinox.

The different steps involved in the data processing include the definition of the ray path for each image (section 2.1), the retrieval of the light curve at each wavelength and for each image (section 2.2), and the inversion of the light curves to retrieve the density profile, scale height, and cross section for each wavelength and for each occultation (section 2.3).

**Table 3:** List of Titan solar occultations to date. The (lat, long) are those of the tangent point for the observation at the end of ingress or beginning of egress.

Flyby #	lat	long W	day
T10 egress	-70	305	1/15/2006
T26 ingress	-75	4	3/10/2007
T32 ingress	-42	96	6/13/2007
T53 egress	2	238	4/20/2009
T62 ingress	-22	235	10/12/2009
T62 egress	-85	51	10/12/2009
T78 ingress	43	156	9/12/2011
T78 egress	35	175	9/12/2011

### 2.1 Ray path for each image – determination of the impact parameter $z_0$

Eight solar occultation observations have been obtained during the first seven years of the Cassini mission (Table 3). These observations have probed Titan's atmosphere at different times and latitudes (Fig.3). The trend from high southern latitudes at the beginning of the mission to high northern latitudes as solstice approaches is related to the inclination of Titan's orbit.

For each occultation, a series of images of the Sun are taken. The VIMS instrument simultaneously acquires intensity measurements in 352 wavelength bands from 0.35- to 5.12- $\mu\text{m}$ . Two scanning mirrors allow us to build an image. Titan's atmosphere scatters and absorbs most of the photons in the VIMS spectral range except in five narrow atmospheric bands centred at 0.933-, 1.082-, 1.270-, 1.590-, and 2.019- $\mu\text{m}$  and two broader atmospheric bands between 2.615- and 2.947- $\mu\text{m}$  and between 4.903- and 5.122- $\mu\text{m}$  [16]. The time of acquisition is the key parameter that is entered in the spice kernels to determine the location of the spacecraft, the position of Titan, and the direction of the Sun (Fig. 4). For each image, the ray path is determined as well as the location of the point closest to Titan called the impact parameter (Fig. 2 and 4).



Equation (1) can be written:

$$\text{Ln}\left(\frac{I_{\text{atm}}(\lambda)}{F_{\text{Sun}}(\lambda)}\right) + \tau_{\text{atm}} = 0 \quad (5)$$

The optical depth ( $\tau_{\text{atm}}$ ) can be expressed as a function of the scattering cross section ( $\sigma_{\text{scat}}$ ) and the density of the scatterers ( $n$ ) that depends on the altitude ( $z$ ):

$$\tau_{\text{atm}} = \sigma_{\text{scat}}(\lambda) \int_{-X_0}^{X_0} n(z) dl \quad (6)$$

The integration is performed along the ray path from the point  $-X_0$  where the ray path enters the atmosphere and the point  $X_0$  where it leaves the atmosphere (Fig. 2).  $X_0$  is expressed by:

$$X_0 = R \sqrt{2 \frac{H - z_0}{R}} \quad (7)$$

where  $R$  and  $H$  are Titan's radius and its atmosphere thickness, respectively (Fig. 2). In equation (6),  $l$  is the distance along the ray path ( $-X_0 < l < X_0$ ). The altitude  $z$  is related to the distance  $l$  by:

$$z = R \left[ \sqrt{1 + 2 \frac{z_0}{R} + \frac{l^2 + z_0^2}{R^2}} - 1 \right] \quad (8)$$

The density of aerosols ( $n$ ) is approximated by an exponential law:

$$n(z) = n_{\text{ref}} \cdot \exp\left(-\frac{z - Z_{\text{ref}}}{H_{\text{haze}}}\right) \quad (9)$$

where  $H_{\text{haze}}$  is the scale height and  $Z_{\text{ref}}$  is a reference altitude where the density of aerosols is  $n_{\text{ref}}$  [5]. A reference altitude of 80 km is chosen. Analysis of the Huygens probe observations during its descent suggests that the number density is constant [5] below that altitude. This result is discussed in section 4.1.

The distribution given by equation (9) gives an analytical solution for equation (6) which can be included into equation (5) which becomes:

$$\text{Ln}\left(\frac{I_{\text{atm}}(\lambda)}{F_{\text{Sun}}(\lambda)}\right) + n_{\text{ref}} \sigma_{\text{scat}}(\lambda) H_{\text{haze}} \exp\left(-\frac{z_0 - Z_{\text{ref}}}{H_{\text{haze}}}\right) \sqrt{2\pi \left(\frac{R}{H_{\text{haze}}} + \frac{z_0}{H_{\text{haze}}}\right)} = 0 \quad (10)$$

The data are  $(\text{Ln}(I/F), z_0)$ . The two parameters that we can invert are the scale height  $H_{\text{haze}}$  and  $(n_{\text{ref}} \cdot \sigma_{\text{scat}})$  since we cannot separate the cross-section from the number density. As discussed in section 4, other observations provide information on the density, which allows us to give information on the cross section. Each solar occultation observation provides information on the haze scale height and the product of reference density by cross section at each wavelength. We use  $(I/F)$  values for the wavelengths where the atmospheric molecules do not absorb (Fig. 6).

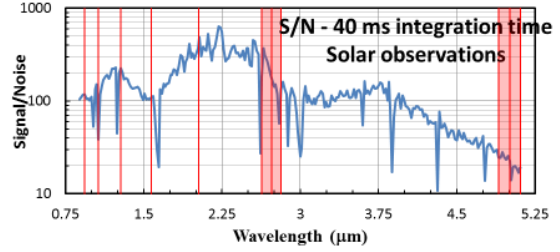


Fig. 6: Signal to Noise ratio for an integration time of 40 ms. The atmospheric windows are identified as vertical red lines. The two wider windows at longer wavelengths are highlighted in light red.

We use an inversion method [17] which has been developed for solving non-linear equations using the least-squares criteria. Data and parameters are put together in a vector column  $X_0$ . Be  $n$  the number of images, the column vector  $X_0$  has  $2n+2$  components. We also enter the covariance matrix  $C_0$  which contains variance on the data (see below) and an a-priori variance on the parameters. If we have no information on the parameters, then the variance is set to a very large value. The algorithm provides the final vector  $X$  through an iterative process:

$$X_{k+1} = X_0 + C_0 F_k^T (F_k C_0 F_k^T)^{-1} [F_k (X_k - X_0) - f(X_k)] \quad (11)$$

where  $F_k$  is the matrix of partial derivatives and  $f(X_k)$  is equation (10). Convergence requires a few iterations.

The standard deviation on the impact parameter is estimated as a quarter of the difference in the value of the impact parameter between two consecutive images. For the standard deviation on  $\text{Ln}(I/F)$ , we use the information coming from the observations of the solar spectrum for impact parameters larger than 1500 km. For each wavelength, we determine the average value of tens of observations and the associated standard deviation. The ratio of the standard deviation by the mean value gives us the S/N ratio (Fig. 6). This information also identifies the bad spectels. The spectels in the atmospheric windows of interest are

identified in Table 1. The standard deviation ( $\sigma$ ) on  $\ln(I/F)$  is determined for each observation using the following equation:

$$\sigma_{\ln(I/F)} = \frac{\sigma_I}{I} + \frac{\sigma_F}{F} = \frac{1}{S/N} \left[ 1 + \frac{1}{I/F} \right] \quad (12)$$

where we assume that the standard deviation on the received spectral radiance is equal to that obtained without atmospheric scattering. A large value of the impact parameter leads to a standard deviation twice the inverse of the S/N. As the value of the impact parameter gets smaller, the value of  $I/F$  also gets smaller and the standard deviation becomes larger.

The a-posteriori covariance matrix is calculated using the following expression [17]:

$$C = C_0 - C_0 F^T (F C_0 F^T)^{-1} F C_0 \quad (13)$$

from which one can extract the standard deviation on each parameter and the correlation matrix: This approach is now used to provide constraints on the cross-section and density of Titan's aerosols from observations obtained during flybys T10 and T53.

Table 4: Results for the T10 occultation. The number in parenthesis is the standard deviation in km for the third column and on the last digit for the fourth column.

spectel #	wavelength	H <sub>haze</sub>	n <sub>ref</sub> . $\sigma$
	micron	km	km-1
100	0.9331	74.9 (1.3)	9.5 E-3 (5)
107	1.0476	73.3 (1.2)	8.0 E-3 (4)
109	1.0818	71.3 (1.2)	7.9 E-3 (4)
121	1.2781	68.3 (0.8)	6.9 E-3 (2)
139	1.5736	71.4 (1.2)	4.0 E-3 (2)
166	2.018	61.6 (0.6)	2.92 E-3 (6)
167	2.034	59.5 (0.5)	2.95 E-3 (6)
203	2.63	64.5 (0.8)	2.17 E-3 (5)
206	2.681	62.4 (0.8)	1.91 E-3 (4)
209	2.733	62.3 (0.9)	1.78 E-3 (4)
212	2.781	67.6 (1.2)	1.43 E-3 (4)
344	4.989	45.9 (5.5)	0.82 E-3 (8)
D2	203:214	65.7 (0.6)	1.77 E-3 (3)
D3	339-352	49.1 (1.6)	0.82 E-3 (3)

### 3. RESULTS

The results for two flybys are described in this section. The first flyby T10 has already been processed [4] and serves as a benchmark for testing the validity of our approach. The second flyby (T53) probes the atmosphere at (2°N, 238°W) which is very close to the

Huygens landing site. The present results on T53 can then be compared with those obtained by [5].

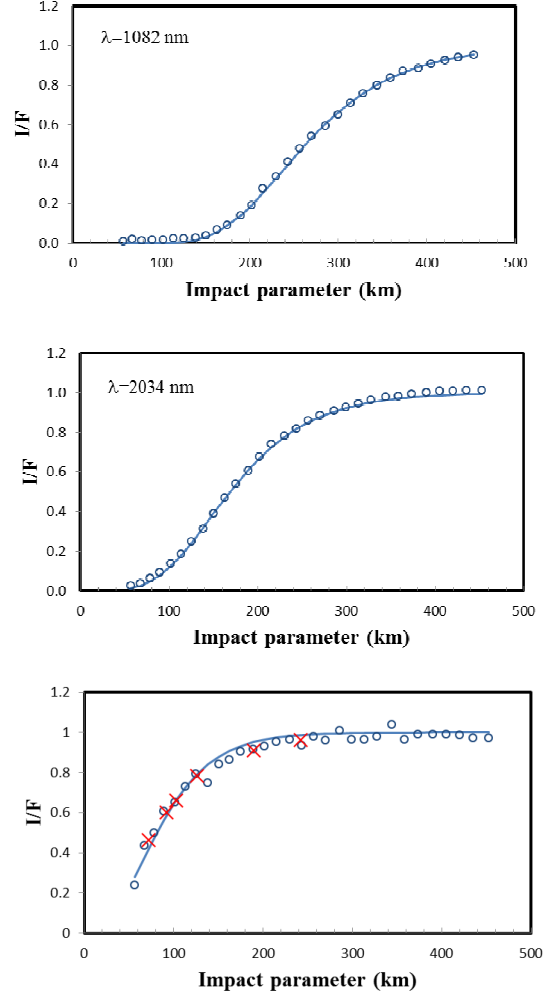


Fig. 7: Comparison between the data (circles) and the fit (solid line) by equation (10) for three wavelengths for the T10 flyby. The red crosses in the lower panel are the values from [4]. Note that each wavelength probes different altitudes from the surface at 5  $\mu$ m to 500 km at 1  $\mu$ m (see text for more details).

#### 3.1 T10 flyby

This flyby occurred in January 2006, during Titan's winter. It probed the atmosphere above the South Pole (Fig. 4) around (70°S, 308°W). The integration time was set to 40 ms. The images are 12 lines by 12 samples. The time between two images is therefore around 7 seconds. Consequently, the impact parameter (Fig. 2) varies by about 7 km between two consecutive images. During this observation, there was no light coming from the boresight of the VIMS

instrument because the secondary axis could be aligned in a direction that prevents this effect.

The fit to equation (10) is shown for three wavelengths from 1  $\mu\text{m}$  to 5  $\mu\text{m}$  (Fig 7). It shows the quality of the fit. The values of the parameters are given in Table 4. Each wavelength probes a different atmospheric layer which can be defined as the layer comprised between the two impact parameters corresponding to values of I/F of 5% and 95%. At small wavelength, the photons are much more scattered that at long wavelength. Therefore the 1- $\mu\text{m}$  bands are sensitive to the atmospheric layer between 160 and 500 km. The signal of the 2- $\mu\text{m}$  band has most of its variations between 80 km and 220 km. The 5- $\mu\text{m}$  photons are not very sensitive to the aerosols and most of the signal varies between the surface where the value is not equal to 0 and about 180 km. The fact that different wavelengths probe different altitudes must be kept in mind when discussing the results.

The scale height varies from 50 km at 5- $\mu\text{m}$  to 75 km at 0.933- $\mu\text{m}$ . It is equal to 70 km, 60 km, and 65 km for wavelengths of -1 to 1.5- $\mu\text{m}$ , 2- $\mu\text{m}$ , and 2.7 $\mu\text{m}$ , respectively. These differences are the result of each wavelength being sensitive to a specific atmospheric layer. Previous work [4] proposed a single scale height of 60 km which is in agreement with the present results although the present study suggests variations as a function of altitude (see section 4.1).

The other parameter is the product of a reference number density of particles at  $Z_{\text{ref}}=80$  km by the cross-section. Since the cross-section strongly decreases with increasing wavelength, it is not surprising to see that the value drops by one order of magnitude between 1- $\mu\text{m}$  and 5 $\mu\text{m}$  (Table 4). The values are discussed in section 4.2 where a comparison is made between the results at the pole and those at the equator.

### 3.2 T53 flyby

This flyby occurred in April 2009, just before the equinox. It probed the atmosphere above the equator on the anti-Saturn hemisphere (Fig. 8) in an area where the atmospheric conditions are very close to those prevailing at the Huygens Landing Site (10.5°S, 192.2°W). The integration time was set to 20 ms. Each image is taken every 2 seconds compared to 7 seconds for the T10 data. It provides a better resolution in altitude (5 km) but a lower S/N for each image. Also, a spectral mask was applied and the values of the last 8 spectels are not available. The spectral summing at 5- $\mu\text{m}$  can be done on 6 spectels instead of 14 but the improvement is still significant (Fig. 9). Finally, reflected light by Titan came into the boresight just after egress for about one minute, which corresponds to impact parameter from 0 to 150 km.

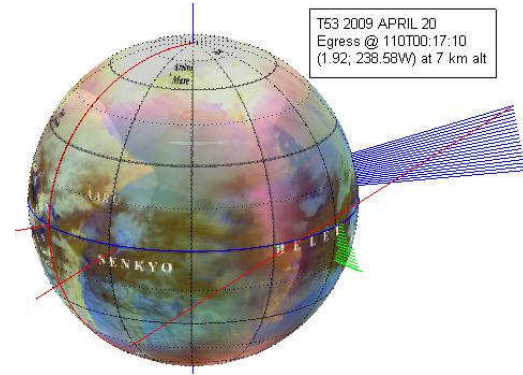


Fig. 8: Geometry of the T53 egress- See caption in Fig.4 for the explanations of the different lines.

Table 5: Results for the T53 observation

spectel #	wavelength	H <sub>haze</sub>	$n_{\text{ref}} \cdot \sigma$
	micron	km	km-1
100	0.9331	34.5	3.22E-01
107	1.0476	34.4	2.53E-01
109	1.0818	35.1	2.14E-01
121	1.2781	40.8	6.40E-02
139	1.5736	47.2	2.13E-02
166	2.018	53.9	7.00E-03
167	2.034	55.3	6.22E-03
203	2.63	66.0 (0.9)	2.96E-03 (7)
206	2.681	65.4 (0.9)	2.62E-03 (7)
209	2.733	64.6 (0.6)	2.42E-03 (4)
212	2.781	66.1 (0.9)	2.19E-03 (5)
344	4.989	63.5 (3.3)	7.58E-04 (3)
D2	203:214	61.1 (0.4)	2.74E-03 (3)
D3	339-344	58.7 (2.7)	8.40E-04 (2)

The fit by equation (10) is presented in Fig. 9 for three wavelengths and the spectral summing at 5- $\mu\text{m}$ . The fit is quite good at each wavelength. The 1- $\mu\text{m}$  wavelength probes a layer between 225 and 340 km, which is deeper than the layer probed by the same wavelength during the T10 flyby. Also the scale height is much smaller, on the order of 35 km (Table 5). At 2- $\mu\text{m}$ , the layer is between 100- and 300 km with a scale height of 55-km. At 5- $\mu\text{m}$ , the atmosphere is probed between the surface and 200 km with a scale height of 60 km. One can note that at 2.7- $\mu\text{m}$ , the scale height is 65 km, close to the one obtained for the T10 data. There is one major difference with the T10 flyby which is the value of the scale heights as discussed in section 4.1. On the other hand, the inverted values for the 5- $\mu\text{m}$  band are quite similar, suggesting that the properties of the aerosols in the troposphere are the same at the equator and at the South Pole.

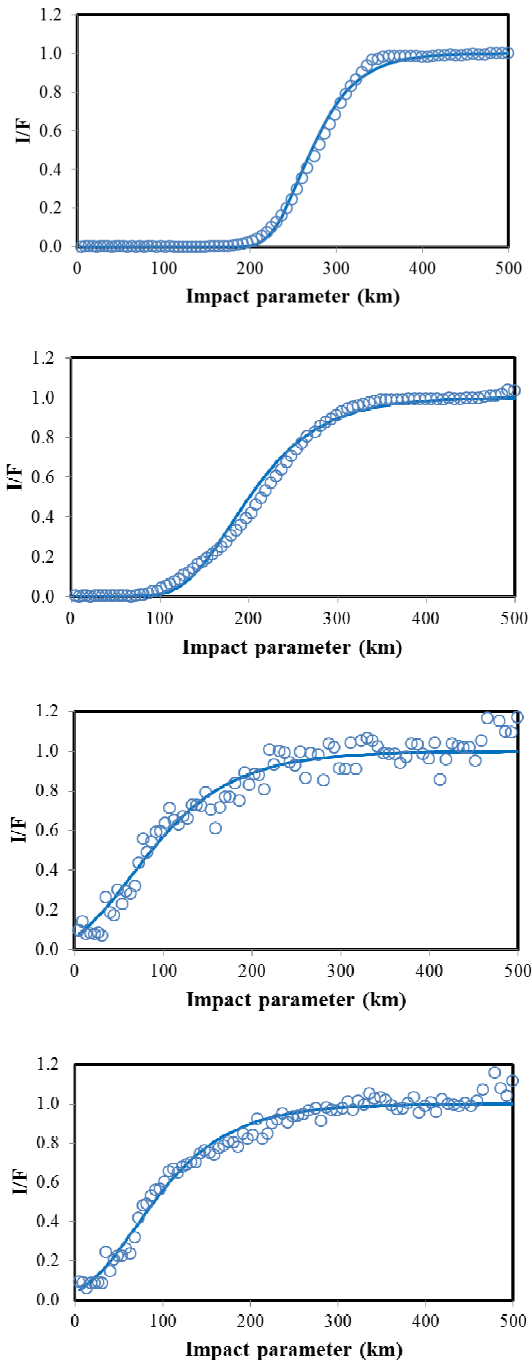


Fig. 9: Comparison between the data (circles) and the fit (solid line) by equation (10) for three wavelengths for the T53 flyby. Note the improvement in the spectral summing at 5- $\mu\text{m}$  although only 6 spectels are available

#### 4. IMPLICATIONS FOR TITAN

Using these two data sets that probe the South Pole and the equatorial region allows us to investigate the implications for the aerosol profile in Titan's atmosphere and the opacity of the atmosphere at different wavelengths.

##### 4.1 Density of aerosols

The results described in section 3 show that each wavelength probes a different part of the atmosphere. The results are summarized in Fig. 10. As expected, longer wavelengths probe deeper in the atmosphere. At 1- $\mu\text{m}$ , the atmospheric probe layer centred around 300 km absorbs most of the light. At 5- $\mu\text{m}$ , the values is equal to 80 km. These two values are the same for both observations. However, one can note that at 2- $\mu\text{m}$ , the sampled layer is deeper for T10 than for T53.

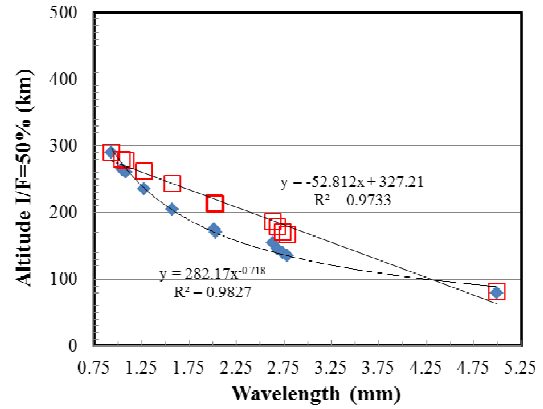


Fig. 10: Values of the impact parameter for which  $I/F=50\%$  as a function of the wavelength for T10 (blue diamonds) and for T53 (red empty squares).

Another implication of the results obtained in section 3 is that the scale height varies with wavelength. And since wavelength gives information on the altitude, one can deduce the scale height versus altitude (Fig. 11). It is quite interesting to note that the two flybys exhibit two different patterns. For the equatorial occultation (T53), the scale height seems constant ( $\sim 65$  km) up to 180 km and then decreases down to 35 km at an altitude of 300 km. On the other hand, for the polar occultation T10, the scale height increases from 45 km at the surface to 75 km at 300 km altitude (Fig. 11). This pattern is consistent with the atmospheric circulation with upwellings at the South Pole during the winter that may stretch the scale height. On the other hand, the fall of particles at the equator

may reduce the scale height. Note that the atmospheric scale height ( $RT/Mg$ ) is equal to 20 km at the surface.

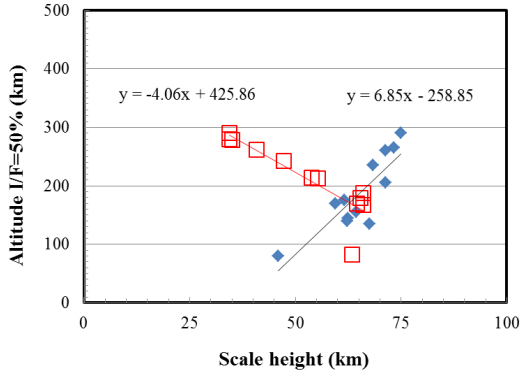


Fig. 11: Relationship between scale height and altitude (see text for explanation). The red squares are for the equatorial occultation and the blue diamonds are the results for the polar occultation.

The notion of scale height is convenient for inverting the data. The inversion of the observations at different wavelengths provides a more precise description of the scale height with altitude. This information is now used to determine the density profile in Titan's atmosphere (Fig. 12) assuming that we know the density at a reference altitude. We use the value inferred from the Huygens probe observations [5] of  $5 \text{ cm}^{-3}$  at a reference altitude of 80 km. The Huygens probe landed in an equatorial area and the number density at 80 km at the pole may be different. However, the inverted value of  $n_{\text{ref}} \cdot \sigma$  for the  $5\text{-}\mu\text{m}$  window is, within the standard deviation, the same for T10 and T53 (Tables 4 and 5). The simplest explanation is that both the reference number density and the cross-section are equal. There is however the possibility that they compensate each other. Such possibility will be discussed in a forthcoming paper when more solar occultation observations will have been processed. With this assumption, one can plot the number density versus altitude (Fig. 12). The curve in a  $(\ln(n), z)$  plot is not linear because the scale height varies with altitude as discussed before. The curves for T10 and T53 intersect at 80 km where the number density is set to  $5 \text{ cm}^{-3}$ . The number density decreases with increasing altitude. It decreases more rapidly for the polar occultation than for the equatorial occultation. That explains why the photons at wavelength between 1- and  $3\text{-}\mu\text{m}$  can penetrate deeper in the atmosphere at the pole than at the equator (Fig. 10).

The value of the vertically integrated amount of aerosols strongly depends on the density profile in the troposphere. Models developed prior to Cassini's arrival at Saturn [19] assumed a relative clearing of the

aerosols below the reference altitude of 80 km. Huygens saw no such clearing and suggests either a constant density or a decrease in density if the particles range in size from 3- to  $10\text{-}\mu\text{m}$  [5]. A constant number density of  $5 \text{ cm}^{-3}$  is shown by the dotted line in Fig. 12. With this value, the vertically integrated value of aerosols is equal to  $70 \cdot 10^6 \text{ particles/cm}^2$ . The difference between the equatorial and polar profile is less than 5%. About 55% of the particles are in the lower 80 km. If the number density keeps increasing with decreasing altitude following the exponential law (Eq. 9), then the integrated value becomes equal to 140- and  $110 \cdot 10^6 \text{ particles/cm}^2$  for the polar and equatorial profiles, respectively. There are more particles in the polar profile because the scale height is smaller by a factor of almost 2.

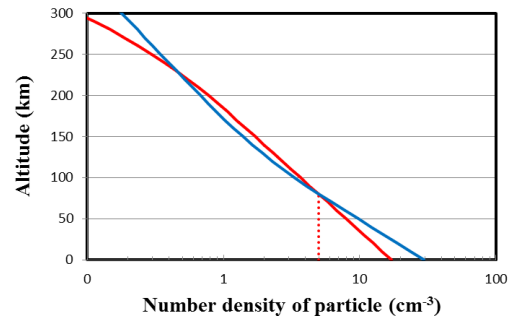


Figure 12: number density of particles assuming a value of  $5 \text{ cm}^{-3}$  [5] at a reference altitude of 80 km. The profiles for T10 (blue) and T53 (red) are then drawn using the scale heights determined in the present study.

## 4.2 Cross-section

For the  $5\text{-}\mu\text{m}$  atmospheric window, the cross section is the inverted value of  $n_{\text{ref}} \cdot \sigma$  divided by the reference number density at 80 km because the photons at this wavelength probe the atmospheric layer at this altitude (Fig. 10). At other wavelengths, a correction is applied such that the reference number density ( $n_{\text{ref},\text{cor}}$ ) and reference altitude ( $Z_{\text{ref},\text{cor}}$ ) correspond to the values where  $I/F$  is 50%:

$$\sigma_{\text{scat}}(\lambda) = \frac{(n_{\text{ref}} \cdot \sigma)_{\text{inv}}}{n_{\text{ref},\text{cor}}} \exp\left(\frac{Z_{\text{ref}} - Z_{\text{ref},\text{cor}}}{H_{\text{haze}}}\right) \quad (14)$$

where the new reference value comes from the profiles determined in section 4.1 (Fig. 12). The cross section can be plotted versus wavelength (Fig. 13). It is remarkable that the two curves are very close to each other. In a log-log plot, the linear trend indicates a power-law dependence. The fit gives power exponent of -1.7 and -1.9 for T10 and T53, respectively. Such power law is predicted for the cross-section [5].

Previous studies [4, 5, 18] found values between -1.3 and -2.3.

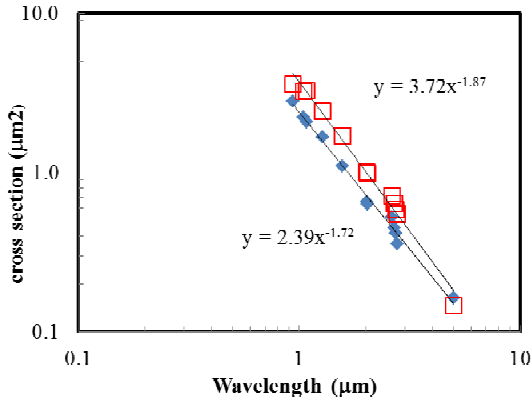


Fig. 13: Cross-section versus wavelength. Blue diamonds are values for the T10 observations (South Pole). Empty red squares are values for the T53 observations (equator). The values at 5- $\mu\text{m}$  are identical.

The very good match between the two curves validates the density profile proposed in section 4.1. However, the two curves are not on top of each other, which suggests that the reference number density may be a little bit different at the pole than at the equator. Studies of other solar occultation observations will provide additional information about the lateral homogeneity of the number density of particles in Titan's atmosphere.

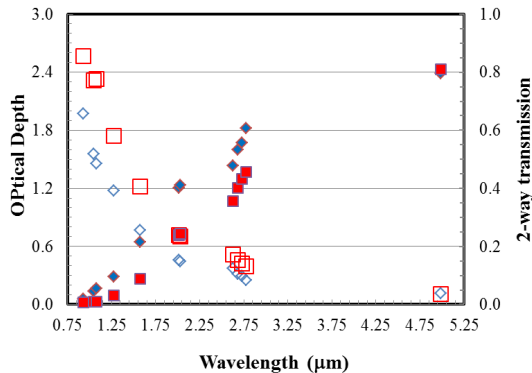


Fig. 14: Optical depth (open symbols) and 2-way vertical transmission (filled symbols) for the polar observations (blue) and equatorial observations (red).

### 4.3 Optical depth and opacity.

In this section, the optical depth and the two-way vertical opacity are calculated. Assuming that the

cross-section is constant with altitude for a given wavelength, the optical depth is the product of the cross section times the vertically integrated number density (section 4.1). The cross-section may vary if particles agglomerate. But the wavelength-dependence described above suggests that it is not the case. The two way vertical transmission is also shown because it illustrates the transparency of the atmosphere at 5- $\mu\text{m}$ .

The results are shown in Fig. 14. The present results suggest that the surface can be barely seen at wavelength lower than 1- $\mu\text{m}$ . Then the transparency increases rapidly with wavelength to reach 80% at 5- $\mu\text{m}$ . We can note that the 2- $\mu\text{m}$  atmospheric window seems more transparent at the pole (40%) than at the equator (25%). On the other hand, the values are quite similar at 5- $\mu\text{m}$ .

One can also note the sharp increase in transmission in the 2.7- $\mu\text{m}$  atmospheric band from 48% at 2.63- $\mu\text{m}$  to 61% at 2.78- $\mu\text{m}$ . This window is critical to the detection of water ice because the water ice spectrum drops dramatically between 2.6- and 2.8- $\mu\text{m}$ . The present data bring some insight into that controversy.

Critical to the observation of the surface is the model of the number density profile in the low atmosphere. In the present model, the density is constant [5]. If the density was to increase according to the scale height, then the integrated number density would be about twice as large and the 2-way transmission would be 40 times smaller. Observations of the surface at different wavelengths [16] clearly show that this is not the case. The VIMS observations confirm the DISR observation that the number density is constant below 80 km. Additional observations and quantitative assessment of the optical depth will provide more information about the transmission properties across Titan's atmosphere.

## 5. CONCLUSIONS

The solar occultation observations by the VIMS instrument show that optical properties of the aerosols are quite similar at the equator and at the pole. Specifically, the density profile and the wavelength-dependence of the cross-section are very similar. These observations demonstrate the strong potential of the 5- $\mu\text{m}$  band where the two-way vertical transmission is as high as 80%. It shows that the transmission at 2- $\mu\text{m}$  varies by a factor 2 between the pole and the equator. Such a large variation has to be accounted for when retrieving the surface reflectance of Titan's surface. They also show the very strong increase in transparency within the 2.7- $\mu\text{m}$  atmospheric window

that is so critical for determining the presence of water ice on Titan's surface.

Future work will include the processing of the other solar occultation observations which will enable us to investigate further variations in latitude and time. Determining the composition of these organic molecules is not possible with the Cassini suite of instruments. Such a determination is important from an astrobiology point of view because Titan's atmosphere is a unique organic factory that helps us to understand the formation of organic molecules in the solar system. Future missions to Titan could carry the relevant instruments to make these critical measurements.

## 6. Acknowledgments

CS acknowledges support by the JPL R&TD program and by NASA Astrobiology Institute. This work has been performed at the Jet Propulsion Laboratory, California Institute of Technology under contract with NASA. Copyright 2012, California Institute of Technology.

## 7. REFERENCES

1. Tobie G. et al., Episodic outgassing as the source of atmospheric methane on Titan, *Nature*, 440, 61-64, 2006.
2. Choukroun M. and Sotin C., Is Titan's shape caused by its meteorology and carbon cycle? *Geophys. Res. Lett.*, 39, L04201, 2012.
3. Griffith C. et al., Evidence for a Polar Ethane Cloud on Titan; *Science*, 313, 1620-1622, 2006.
4. Bellucci A. et al., Titan solar occultation observed by Cassini/VIMS: Gas absorption and constraints on aerosol composition; *Icarus*, 201, 198-216, 2009.
5. Tomasko M.G. et al., A model of Titan's aerosols based on measurements made inside the atmosphere, *Planet. Space Sci.*, 56, 669-707, 2008.
6. Rodriguez S. et al., Titan's cloud seasonal activity from winter to spring with Cassini/VIMS; *Icarus*, 216, 89-110, 2011.
7. Wahlund J.E. et al., On the amount of heavy molecular ions in Titan's ionosphere; *Planet. Space Sci.*, 57, 1857-1865, 2009.
8. LeGall A. et al., Cassini SAR, radiometry, scatterometry and altimetry observations of Titan's dune fields; *Icarus*, 213, 608-624, 2011.
9. Hayes A.G. et al., Hydrocarbon lakes on Titan: Distribution and interaction with a porous regolith; *Geophys. Res. Lett.*, 35, L09204, 2008.
10. LeMouelic S. et al., Dissipation of Titan's north polar cloud at northern spring equinox; *Planet. Space Sci.*, 60, 86-92, 2012.
11. Rannou P. et al., A couple dynamics-microphysics model of Titan's atmosphere; *Icarus*, 170, 443-462, 2004.
12. Toon et al., *Icarus*, 75, 255, 2008.
13. Rannou et al., Titan haze distribution and optical properties retrieved from recent observations, *Icarus*, 2010.
14. Mandt K.E. et al., The 12C/13C ratio on Titan from CASSINI INMS measurements and implications for the evolution of methane; *Ap. J.*, 1017 749:160, 2012.
15. Neish C.D. and Lorenz R.D. Titan's global crater population: A new assessment; *Planet. Space Sci.*, 60, 26-33, 2012.
16. Sotin C. et al., Release of volatiles from a possible cryovolcano from near-infrared imaging of Titan, *Nature* 435, 786-789, 2005.
17. Tarantola A. and Valette B., Generalized Nonlinear Inverse Problems Solved Using the Least Squares Criterion, *Rev. Geophys.*, 20, 219-232, 1982.
18. Sicardy B. et al., The two Titan stellar occultations of 14 November 2003. *J. Geophys. Res. (Planets)* 111, doi:10.1029/2005JE002624. E11S91,
- [19] Rannou P. et al., A model of Titan's haze of fractal aerosols constrained by multiple observations; *Planet. Space Sci.* 51, 963-976, 2003.